Supporting Information

A Flexible Polymer-Based Li–Air Battery Using a Reduced Graphene Oxide/Li Composite Anode

Ziyang Guo,[a] Jinli Li,[a] Yuan Xia,[b] Chao Chen,[a] Fengmei Wang,[a] Andebet Gedamu Tamirat,[b] Yonggang Wang,[b] Yongyao Xia,[b] Lei Wang*[a] and Shouhua Feng[a]*

a Key Laboratory of Eco-chemical Engineering, Ministry of Education, College of Chemistry and Molecular Engineering, Qingdao University of Science and Technology, Qingdao 266042, China.

b Department of Chemistry and Shanghai Key Laboratory of Molecular Catalysis and Innovative Materials, Institute of New Energy, Fudan University. Shanghai 200433, China.

---

* Corresponding author. Tel & Fax: 0086-21-51630318
E-mail address: *inorchemwl@126.com; yyxia@fudan.edu.cn*

Material Preparation

Materials Tetraethylene glycol dimethyl ether (TEGDME, 99.9%) and LiTFSI (Sigma-Aldrich, 99.95%) were purchased from Sigma-Aldrich. N-methyl-2-pyrrolidinone (C_5H_9NO, 99%) were purchased from Aladdin Reagent. Trimethylolpropaneethoxylatetriacrylate (average Mn of ~428), 2-hydroxy-2-methyl-1-phenyl-1-propanone ($C_6H_5COC(CH_3)_2OH$, 97%), and poly(vinylidene fluoride-co-hexafluoropropylene) (average Mn of ~130000) were purchased from Sigma-Aldrich. Other chemicals were from Shanghai Chemical Corp. All chemicals were used as received without further purification.

Synthesis of the reduced graphene oxide Graphene oxide was obtained according to the Hummer method (**ref. S1**). Firstly, the aqueous graphene oxide solution was synthesized according to the modified Hummer method. Briefly, the pristine graphite flakes (2g) was put into the concentrated H_2SO_4 (92 mL) solution containing 2g $NaNO_3$, which was stirred at 0 °C in a water/ice bath. $KMnO_4$ (12 g) was then gradually added and the mixture was continuously stirred at 0 °C for 90 minutes. Subsequently, the ice bath was removed and the beaker was heated to 35 °C and maintained at this temperature for 2 hours, followed by the slow addition of 92 mL of deionized (DI) water. The temperature of the reaction mixture increased to ~98 °C and the reaction vessel was maintained at this temperature for 1 hour. Then, the suspension was further diluted with 300 mL of additional water and treated with 30 % H_2O_2 until the cessation of gas evolution. After that, a suspension of graphite oxides was obtained. The graphite oxides suspension was allowed to settle down and the clear solution at the top was repeatedly removed and replaced with deionized water until the suspension became neutral. Subsequently, the resulting slurry of graphite oxide was subjected to many ultrasonication and centrifugation cycles until no sediment was found at the bottom of the centrifuge tube. Finally, a well-dispersed aqueous graphene oxide solution was synthesized. And then the well-dispersed

aqueous graphene oxide solution was coated on the surface of polyfluortetraethylene plate and dryed at 100 °C for 12 h to obtain the graphene oxide (rGO) film.

Synthesis of SiO_2 nanospheres Monodispersed silica microspheres with diameters of 230 nm were synthesized via modified Stöber method (**ref. S2**). Briefly, tetraethyl orthosilicate (TEOS, 25 mL) was dissolved in ethanol (360 mL) at 25 °C, followed by slowly adding the mixture of ammonium hydroxide (22mL) and deionized water (18 ml). The mixture was kept stirring at 30 °C for 12 h. The diameter of the silica microspheres could be adjusted by varying the amount of TEOS and ammonia hydroxide. After that monodisperse silica microspheres were obtained after centrifugation and dispersion in water for several times to remove the residues. Afterward, the obtained silica spheres, which dispersed in water with a concentration of 5 wt %, were allotted into 10 mL vials.

Ionic conductivity tests Electrochemical impedance spectroscopy measurments of *x* % SiO_2-LiI-GPE were carried out in the frequency ranging from 10 Hz to 1000 kHz using stainless steel sheets (SSS) symmetric cell (SSS/electrolyte/SSS). The tested electrolyte resistance was stemed from the intercept of the Nyquist plot with the real axis. The conductivity σ of the prepared electrolyte membranes was obtained using the following equation:

$$\sigma = l/RS$$

Here, R is the measured resistance of the prepared electrolyte membrane, l is the thickness of the prepared electrolyte membrane between counter SSS electrodes, and S is the contact area of the prepared electrolyte membrane and the electrodes.

Electrode preparation and battery assembly of the convetional Li–air batteries In the preparation of rGO cathode, 90 wt % rGO and 10 wt % polyvinylidene fluoride binder (PVDF) were intimately mixed in a N-methyl-2-pyrrolidone (NMP) solution, and the resulting slurry was coated on a carbon paper. The coated electrode was dried

for 12 h at 100 °C under vacuum to remove residual solvent. The batteries were operated in a glove box filled with pure argon. These two electrodes are separated by a separator dipping with 1 M TEGDME/LiTFSI. This Li/separator/O_2 electrode was then sealed into a Swagelok cell with an air hole 0.8 cm^2 placed on the positive electrode side to allow the oxygen to flow in. The cells were cycled in a LAND cycler Wuhan Land Electronic Co. Ltd. All experiments were carried out in a dry and pure oxygen glove box. All of the results for the specific capacities and current densities were calculated with the total mass of rGO in the cathodes.

Synthesis of SiO_2-GPE 4 g Solution A (1 M LiTFSI in TEGDME), 5 g Solution B (1 g PVDF-HFP/4 g NMP) and 3.01 g Solution C (0.01 g HMPP in 3 g TMPET) were well mixed to form the precursor solution. Finally, the solidified gel electrolytes were achieved after the above mixed soulutions are irradiate by UV light (wavelength of 365 nm) for ~20 s. The obtained gel electrolytes can be denoted as SiO_2-GPE.

Preparation of flexible rGO-based cathode In the preparation of flexible rGO-based cathode, 90 wt % rGO and 10 wt % polyvinylidene fluoride binder (PVDF) were intimately mixed in a N-methyl-2-pyrrolidone (NMP) solution, and the resulting slurry was coated on carbon textiles (1.0*5.0 cm^2). Then, the coated electrode was dried for 12 h at 120 °C to remove residual solvent.

Characterization instrumentation

XRD measurements were performed on a Bruker D8 Focus power X-ray diffractometer with Cu K_α radiation. Field emission scanning electron microscopy SEM investigations were conducted using a JSM-6390 microscope from JEOL. Transmission electron microscopy (TEM) experiments were conducted using a JEOL

2011 microscope (Japan) operated at 200 kV. The surface of as-prepared sample was characterized by Raman spectroscopy (LABRAM-1B). Specific surface areas were calculated by the Brunaure–Emmert–Teller method. Pore volumes and sizes were estimated from the pore-size distribution curves from the adsorption isotherms using the Barrett–Joyner–Halenda method. X-ray photoelectron spectroscopy (XPS) was conducted with a Thermo Escalab 250 equipped with a hemispherical analyzer and using an aluminum anode as a source. Fourier transform-infrared spectroscopy (FT-IR) tests were performed on a Nicolet 6700 spectrometer. The surface of as-prepared sample was characterized by Raman spectroscopy (LABRAM-1B). Power electronic conductivity investigation a the pressure of 4 MPa was performed on a 4-pole conductivity instrument for powder materials (Powder Resistivity Meter, FZ-2010,Changbao Analysis Co., Ltd, Shanghai, China). The TG-DSC measurements were performed using a TGA thermal analyzer (NETZSCH, Germany) at a heating rate of 10 °C/min under a 40 mL/min N_2 flow. LAND cycler (Wuhan Land Electronic Co. Ltd) was employed for electrochemical tests. A quadrupole mass spectrometer (NETZSCH QMS 403 C) with leak inlet was connected to a customized Swagelok cell assembly for DEMS investigation (see **Figure S26** in supplementary information for detail).

Figure S1 Time evolution of Li infusion into GO film.

Figure S1 gives the images of Li infusion process into the GO film after different time (a, 0 s; b, 5 s; c, 10 s; d, 20 s; e, 25 s). As shown in **Figure S1a** and **b**, when the edge of the GO film was put in contact with the molten Li, a drastic reduction reaction occurs on the GO film. Then, rapid Li infusion can be observed where it took less than 1 minute for Li to spread across the whole rGO/Li surface (**Figure S1c-e**).

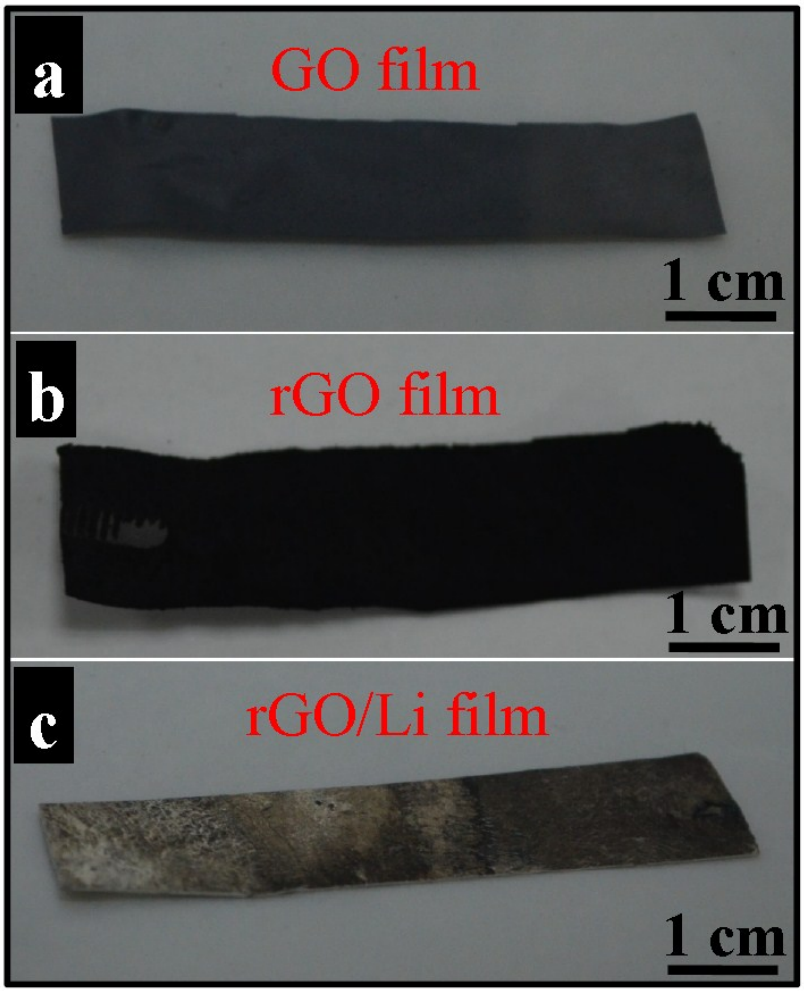

Figure S2 The digital images of (a) the GO film, (b) the rGO film and (c) rGO/Li composite film. The size of these films shown in a–c is ~1*5 cm^2.

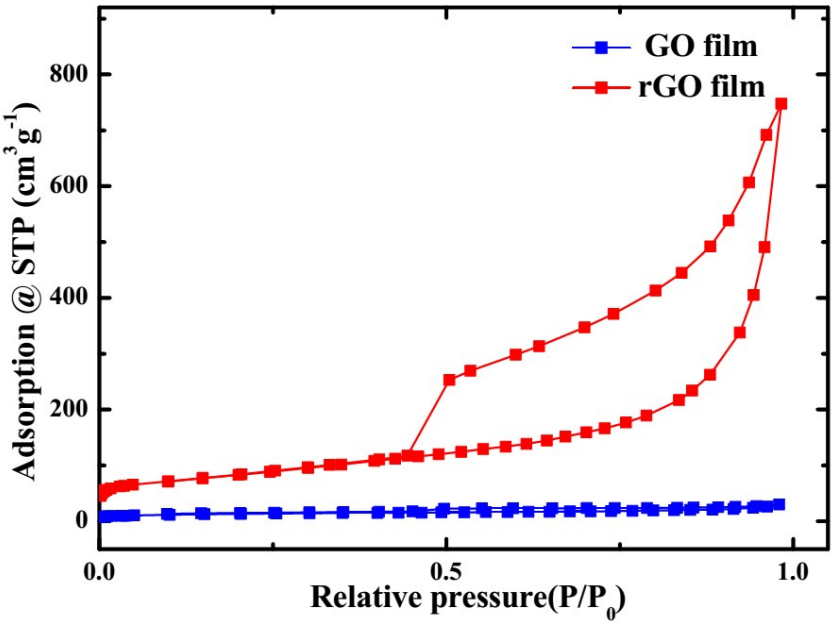

Figure S3 N_2 adsorption/desorption isotherms of the pristine GO film (blue) and the rGO film (red).

It can be detected from **Figure S3** that the porosity of the rGO film obviously increases after the reduction reaction. Moreover, the Brunauer–Emmett–Teller (BET) surface area of the rGO film is 294.5 m^2 g^{-1}, which is much higher than that of pristine GO film (41.9 m^2 g^{-1}).

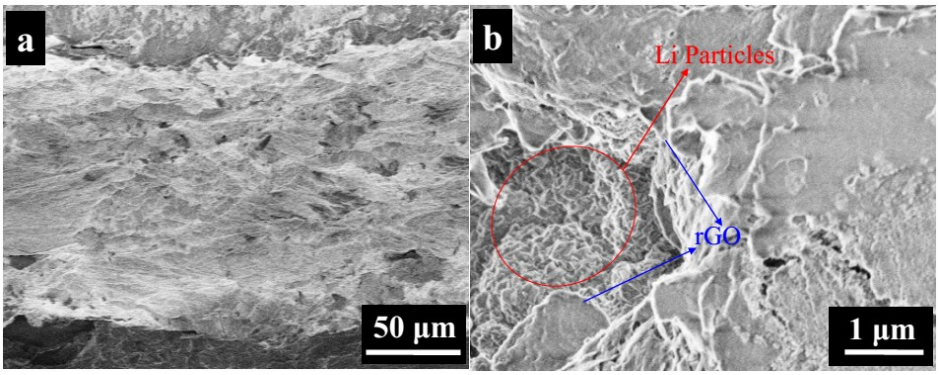

Figure S4 The cross-sectional SEM images of rGO/Li anode with different magnifications.

As shown in **Figure S4**, the rGO/Li anode consists of the Li particles and rGO films. Moreover, it can be further found from **Figure S4b** that the voids between rGO layers are filled with uniform Li particles.

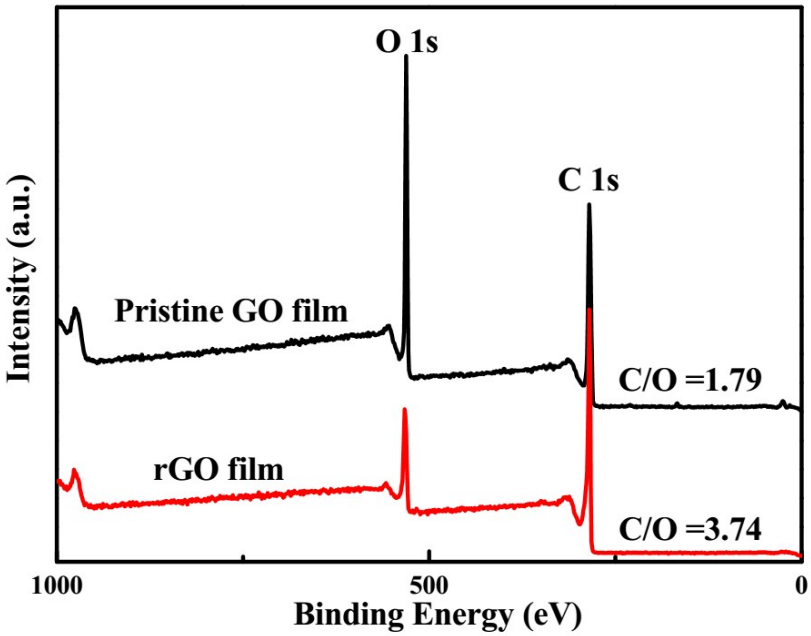

Figure S5 Full XPS spectra of pristine GO film and rGO film.

Figure S5 shows the full XPS spectra of pristine GO film (black) and rGO film (red). As shown in **Figure S5**, after the reduction reaction, significantly increased C/O ratio can be observed, which indicates the removal of O-containing species and the reduction of GO film.

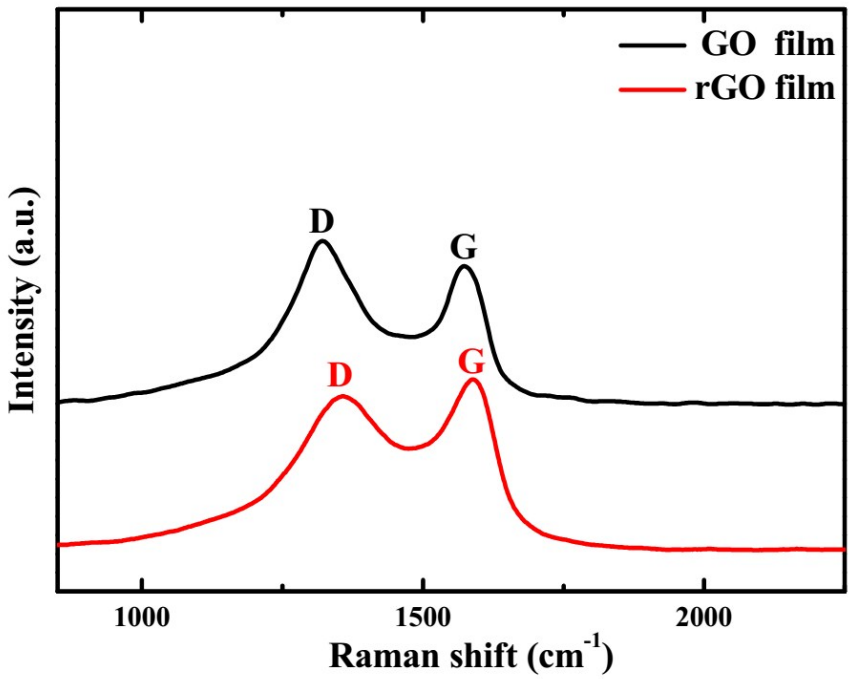

Figure S6 Raman spectroscopy characterizations on the pristine GO film/rGO film.

Figure S6 gives the Raman spectra of pristine GO (black) and rGO (red) films. The rGO film showed lower D/G band ratio than that of GO film, clearly indicating reduction of GO.

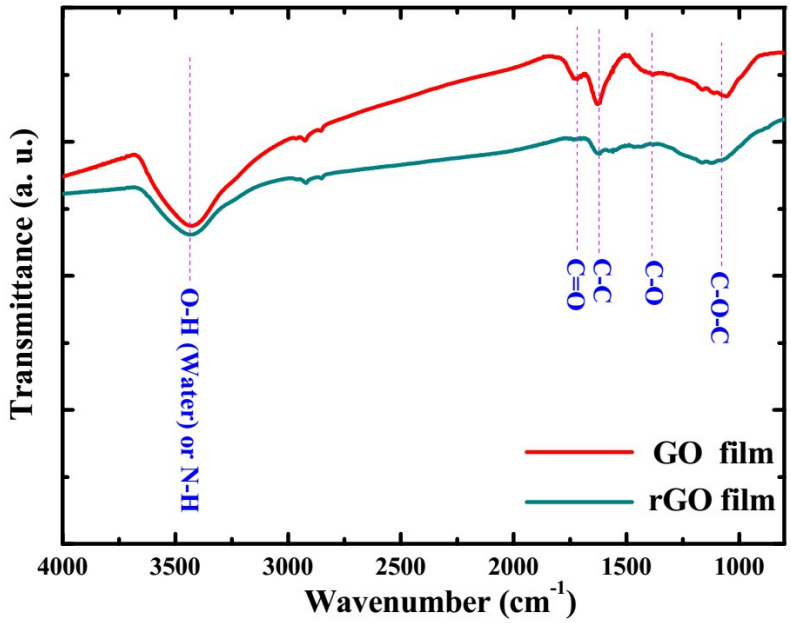

Figure S7 FTIR spectra of a pristine GO film and an rGO film

As shown in **Figure S7**, the GO film exhibits a strong and broad peak around 3,400 cm^{-1} corresponding to –OH stretching, indicating the presence of adsorbed water or surface –OH. Meanwhile, characteristic peaks of other surface groups such as carbonyl (C=O) (~1,740 cm^{-1}) and epoxyl (C–O–C) (~1,050 cm^{-1}) were also observed. In contrast, after the reduction reaction, the abovementioned oxygen-containing functional groups became almost undetectable, confirming the removal of residual water and the high reduction level of GO.

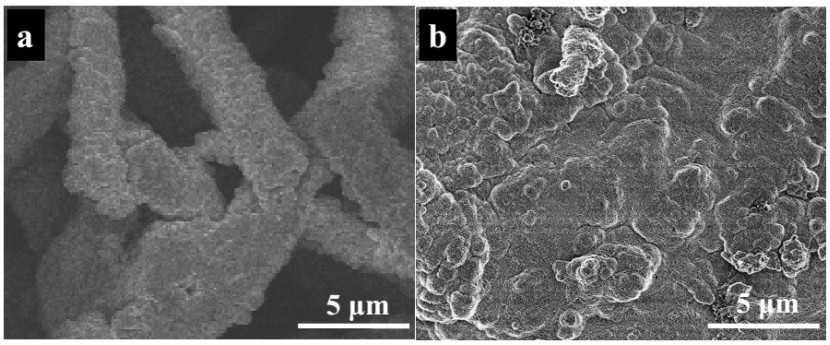

Figure S8 SEM images of (a) the bare Li foil surface and the rGO/Li surface after 100 galvanostatic cycles. The current density was fixed at 1 mA cm^{-2} and the capacity was set at 1 mAh cm^{-2}.

As shown in **Figure S8**, after 100 cycles at 1 mA cm^{-2} with limited capacity of 1 mAh cm^{-2}, the cycled rGO/Li electrode still remains dendrite-free, whereas the cycled Li metal exhibits a more uneven surface with rugged and dendritic Li deposition. These results further demonstrate the excellent Li plating/stripping performance of the rGO/Li anode.

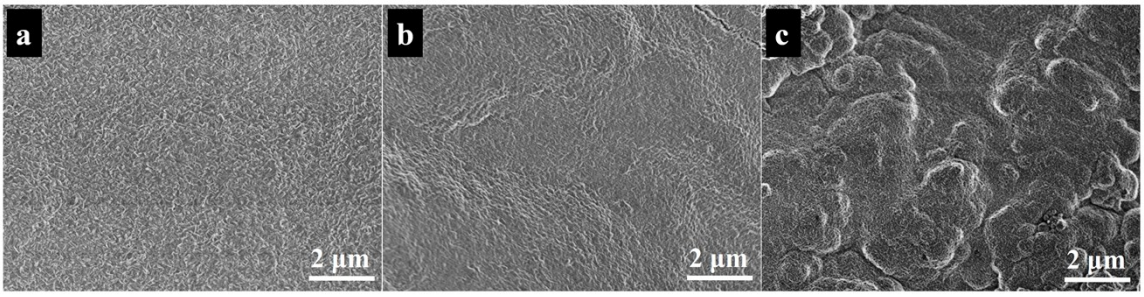

Figure S9 SEM images of the rGO/Li anode at different cycles: (a) before cycling, (b) after 25 galvanostatic cycles and (b) after 100 galvanostatic cycles. The current density was fixed at 1 mA cm^{-2} and the capacity was set at 1 mAh cm^{-2}.

As shown in **Figure S9a**, the surface of the pristine rGO/Li anode is very smooth. After 25 cycles, the cycled rGO/Li electrode still remains flat and dendrite-free (**Figure S9b**). However, the cycled rGO/Li anode shows an uneven surface after 100 cycles, but there is still no dendritic Li formed on its surface (**Figure S9c**). These images during cycling also confirm the excellent Li plating/stripping performance in the rGO/Li anode.

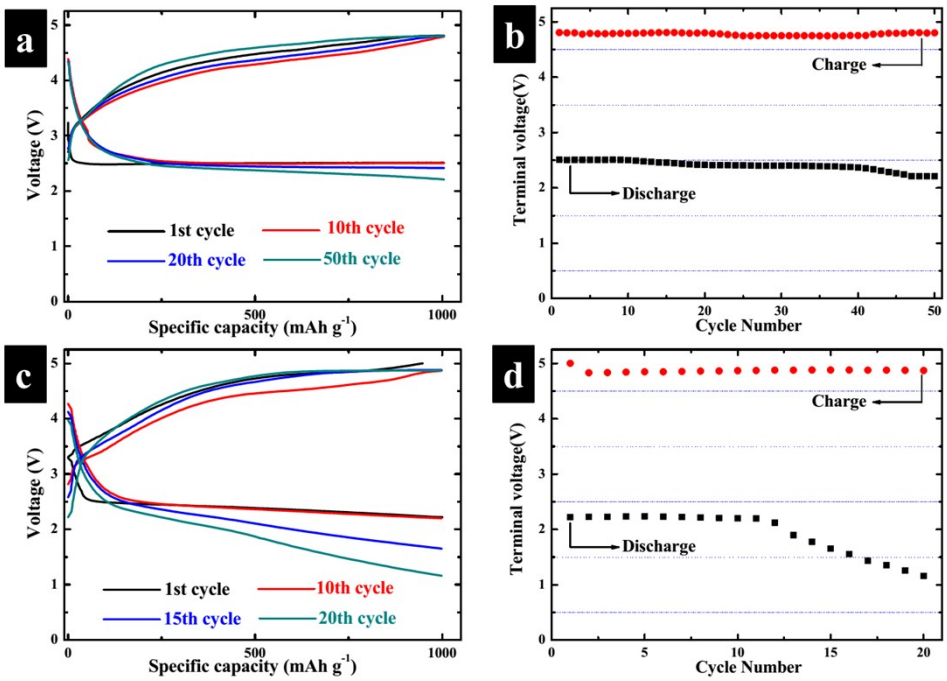

Figure S10 Discharge/charge curves at different cycles and variation of voltage on the terminal of discharge of the rGO/Li based Li–air battery (a, b) and the metallic Li based Li–air battery (c, d).

As shown in **Figure S10a**, the rGO/Li based Li–air battery shows almost reproducible voltage curves with no capacity fade for 50 cycles. Furthermore, the voltages obtained at the discharge terminal of the rGO/Li based Li–air battery are higher than 2.2 V over 50 cycles (**Figure S10b**). In contrast, the terminal discharge voltages of the metallic Li based Li–air battery (**Figure S10c** and **d**) degrades to＜2.0V after only 12 cycles. Obviously, the cycle performance of the rGO/Li based Li–air battery is much better than that of the Li–air battery using fresh Li anode, which can be attributed to the superior Li plating/stripping performance of the rGO/Li anode.

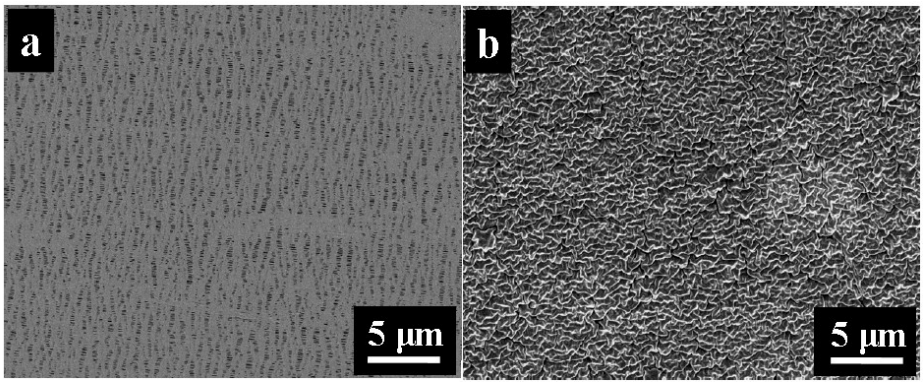

Figure S11 SEM images of (a) celegard membrane wetted by liquid electrolyte (1 M LiTFSI-TEGDME) and (b) gel polymer electrolyte containing 0.05 M LiI (LiI-GPE).

As shown in **Figure S11a**, the surface of celegard membrane presents many elliptic micropores. It can be detected from **Figure S11b** and **Figure 3c** that the LiI-GPE and 4 % SiO_2-LiI-GPE exhibit typical solid state morphology without obvious micropores in the bulk, which is different from that of celegard membrane

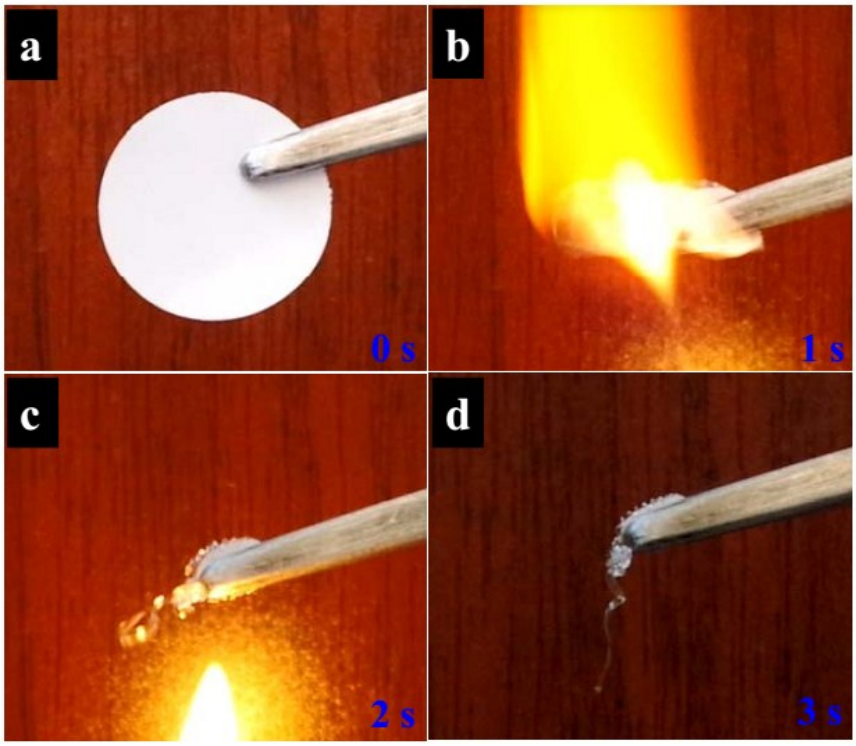

Figure S12 Inflammability test of celegard membrane before loading with liquid electrolyte. Fire from a lighter is ~500°C.

As shown in **Figure S12**, the celegard membrane shrinks rapidly and is entirely burned out in a very short time of <3 s.

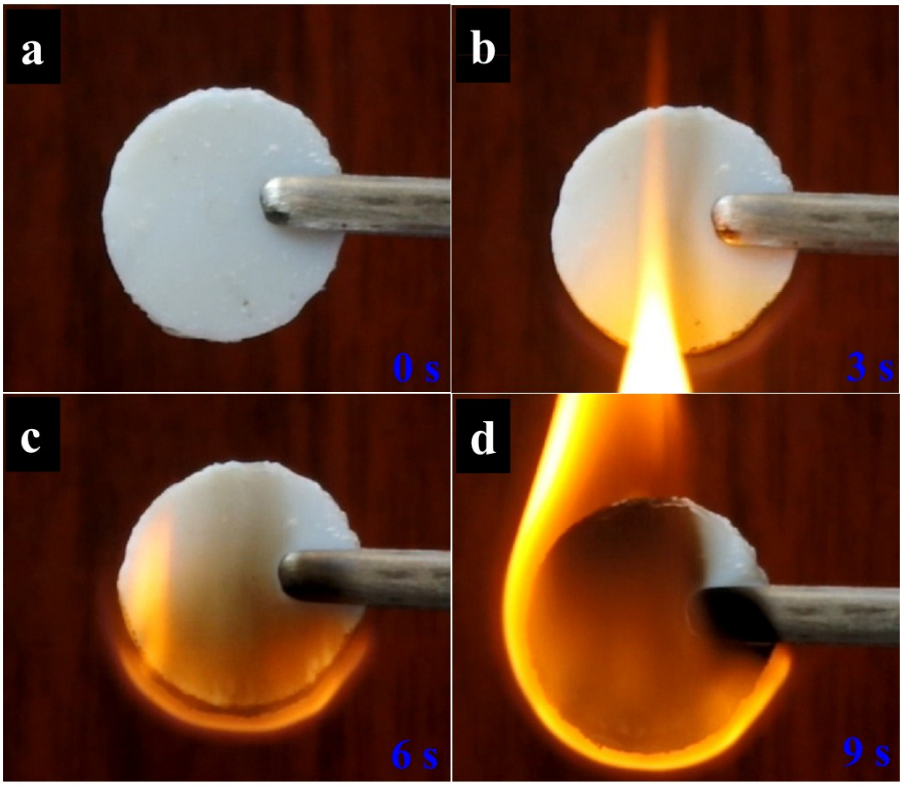

Figure S13 Inflammability test for the polymer matrix of LiI-GPE before loading with liquid electrolyte. Fire from a lighter is ~500°C.

As shown in **Figure S13**, the polymer matrix of LiI-GPE catches fire soon and even continues to burning without ceasing.

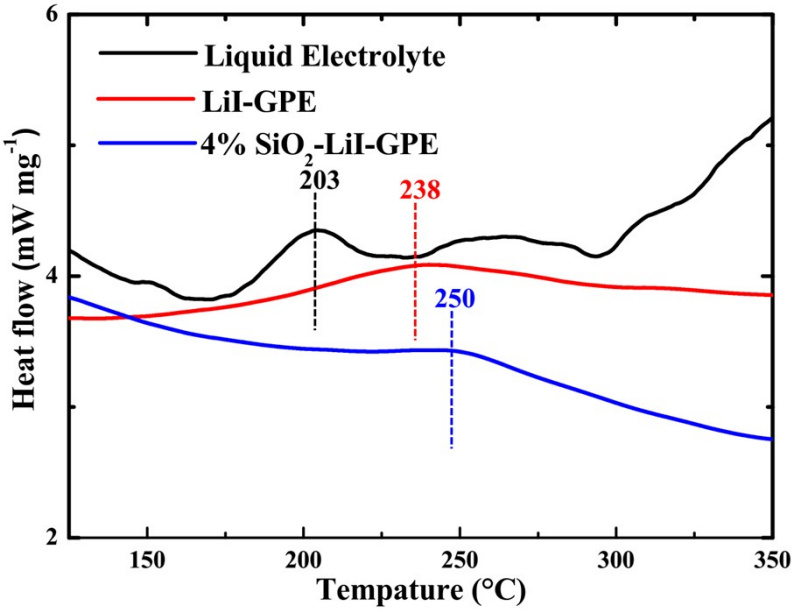

Figure S14 The heat flow curves of 4 % SiO_2-LiI-GPE, LiI-GPE and conventional separator (celegard membrane) wetted by liquid electrolyte (1 M LiTFSI-TEGDME solution).

As shown in **Figure S14**, it can be observed from the heat flow curves of three electrolytes that the endothermic peak at 203 °C for celegard membrane wetted by liquid electrolyte corresponds to the electrolyte evaporation, while it shifts to 238 °C for LiI-GPE and 250 °C for 4 % SiO_2-LiI-GPE, well consistent with the TGA results (**Figure 3e**).

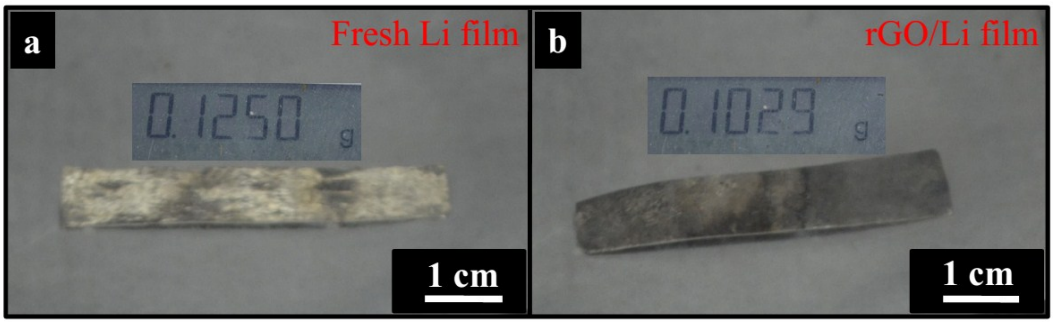

Figure S15 The digital camera images of (a) the fresh Li film and (b) the rGO/Li composite film. The size of both films is ~1*5*0.08 cm^3.

As shown in **Figure S15**, the volumes of the fresh Li film and the rGO/Li composite film are almost the same, but their weight is different. It can be obvesered that the total weight of rGO/Li composite film is only 102.9 mg which is ~18 wt% lighter than the same size of the fresh Li film (125.0 mg), indicating that the introduction of GO can obviously reduce the mass of this Li-based anode

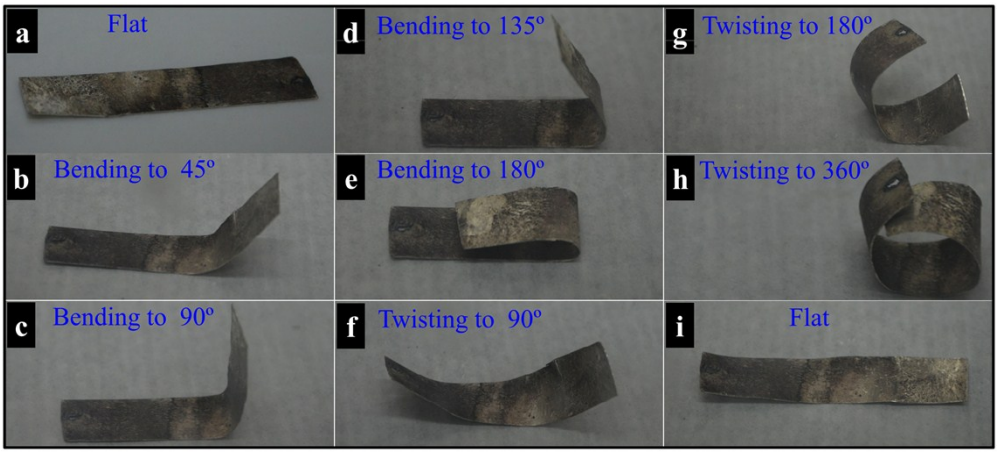

Figure S16 The flexible properties of the rGO/Li composite film at different bending and twisting conditions.

As shown in **Figure S16**, before and after undergoing a series of deformations, including bended at degrees of 45°, 90°, 135°, 180° and twisting to 90°, 180°, 360°, the rGO/Li composite film is almost unchanged, suggesting the high mechanical strength and flexibility of the rGO/Li anode.

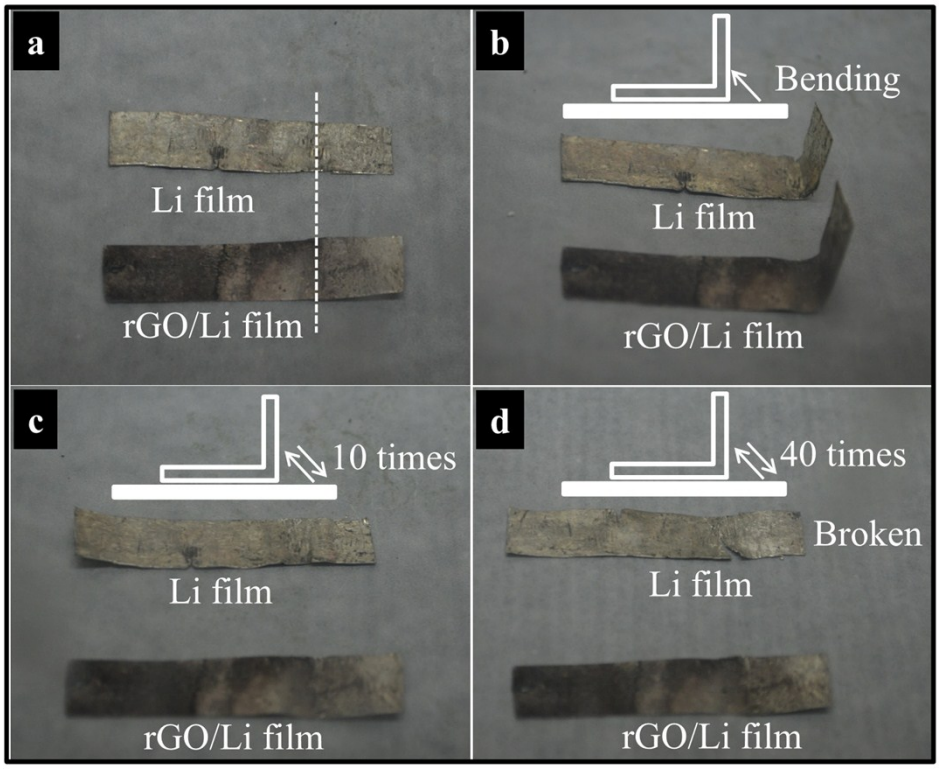

Figure S17 Toughness test, we use two tweezers to bend the Li film and rGO/Li composite film.

As shown in **Figure S17**, both pure Li belt and rGO/Li belt are bended for dozens of times. The pure Li belt is broken after bending for 40 times; while, the rGO/Li belt is still intact, suggesting that rGO film improves the toughness of rGO/Li anode.

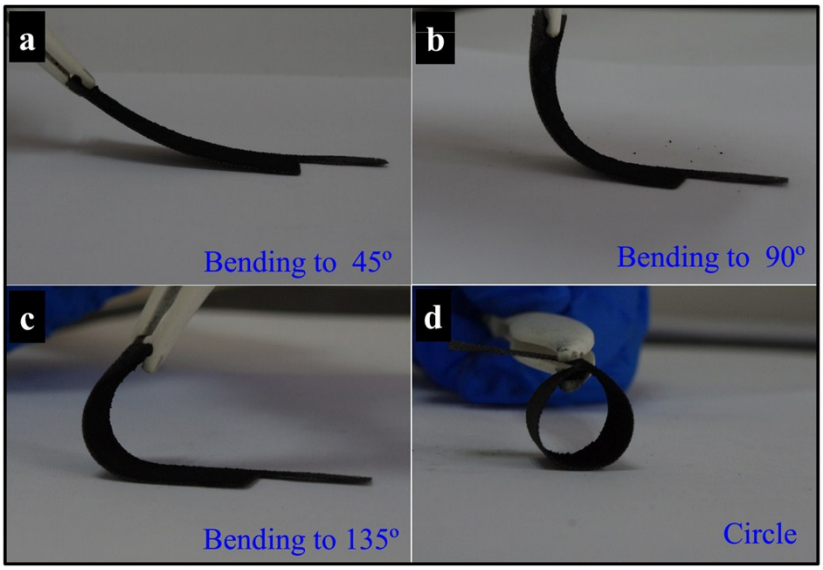

Figure S18 Photo images of rGO-based cathode at different bending conditions.

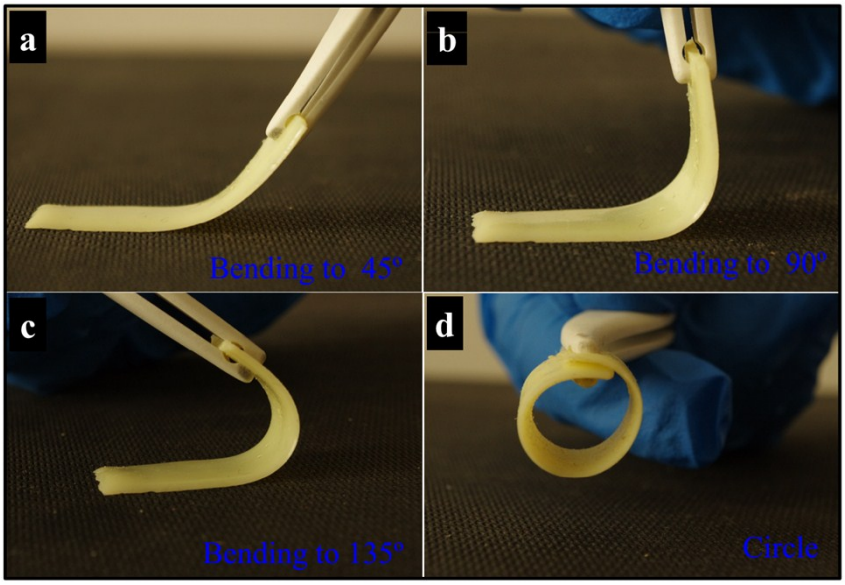

Figure S19 Toughness test, we use the tweezer to bend the 4 % SiO_2-LiI-GPE film.

As shown in **Figure S18** and **19**, both the rGO-based cathode and the 4 % SiO_2-LiI-GPE film exhibit superior flexibility and high mechanical strength since they can be bent at different shapes without damage in structure.

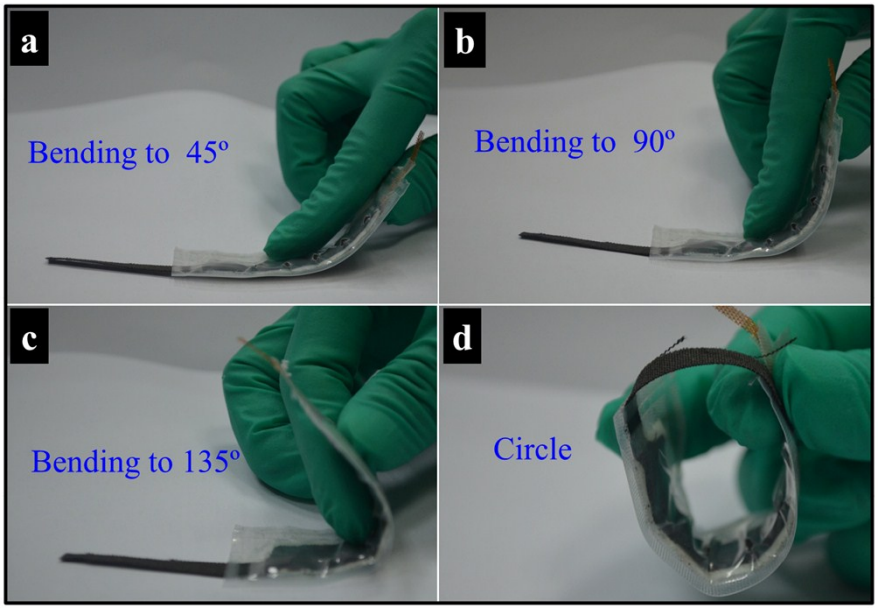

Figure S20 Photo images of the Li–air battery with rGO/Li anode using 4 % SiO_2-LiI-GPE at different bending conditions: bended at degrees of (a) 45°, (b) 90°, (c) 135° and (d) bended to a circle.

Figure S20 indicates that the Li–air battery with rGO/Li anode using 4 % SiO_2-LiI-GPE exhibits high mechanical strength and integrity after undergoing different bending conditions.

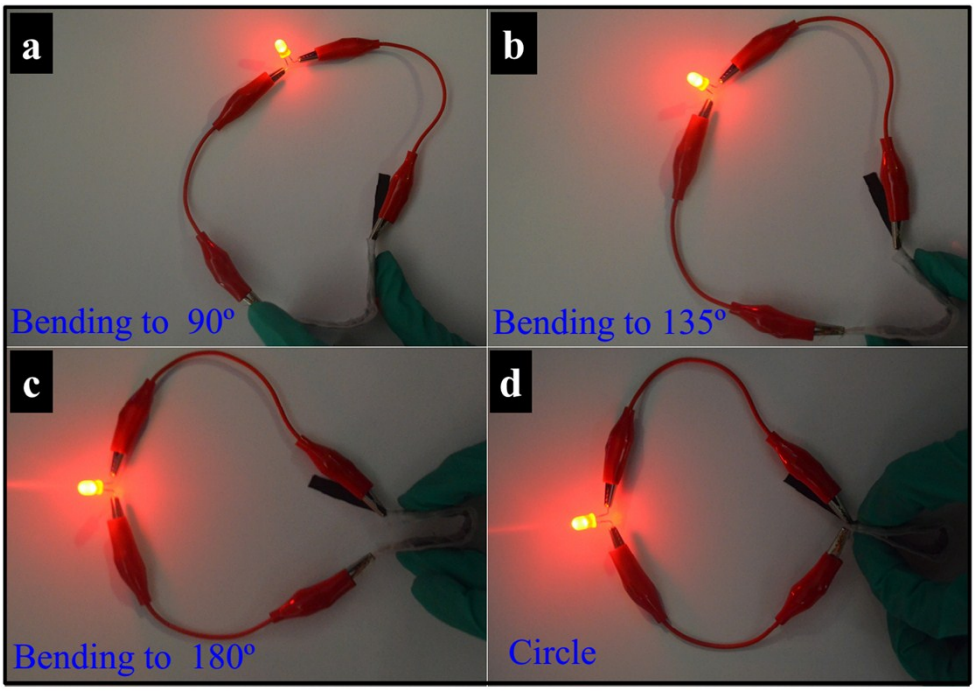

Figure S21 Photo profile of a LED driven by a belt-shaped Li–air battery using 4 % SiO_2-LiI-GPE with rGO/Li anode at different bending conditions: bended at degrees of (a) 90º, (b) 135º, (c) 180º and (d) bended to a circle.

Figure S21 indicates that the Li–air battery with rGO/Li anode using 4 % SiO_2-LiI-GPE exhibits high mechanical strength and integrity after undergoing different bending conditions.

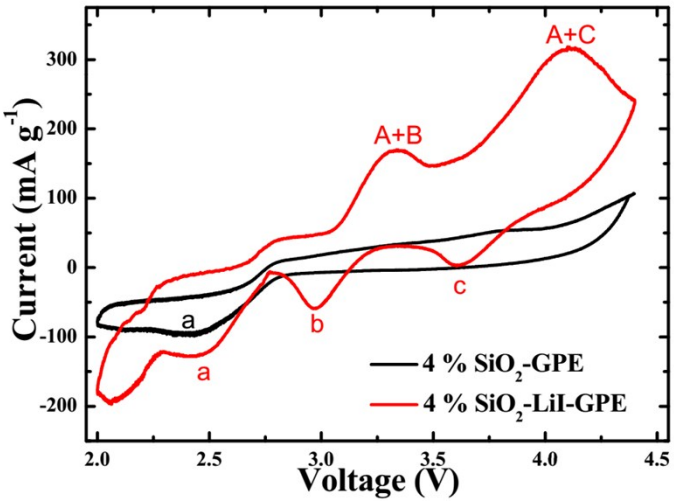

Figure S22 CVs of the Li–air batteries with the two types of electrolytes at a constant scan rate of 0.2 mVs^{-1}: 4 % SiO_2-GPE (black line) and 4 % SiO_2-LiI-GPE (red line).

As shown in **Figure S22**, the Li–air battery using 4 % SiO_2-GPE shows a broad cathodic peak (black $peak_a$) centered around 2.5 V which corresponds to oxygen reduction reaction (ORR). However, there are no obvious anodic peak over charge process for the Li–air battery using 4 % SiO_2-GPE. This phenomenon indicates the reactions of the Li–air battery using 4 % SiO_2-GPE over the discharge/charge process are not totally reversible. In addition, the Li–air battery using 4 % SiO_2-LiI-GPE also exhibits typical ORR peak (red $peak_a$) centered around 2.5 V. Moreover, the Li–air battery using 4 % SiO_2-LiI-GPE further presents the two sets of peaks (red $peak_b$+$peak_{A+B}$ and red $peak_c$+$peak_{A+C}$) centering around 3.3 and 3.8 V, which should be mainly assigned to the I_3^-/I^- and I_2/I_3^- redox couples, respectively. This phenomenon is in agreement with previous report (**ref. S4**). However, it should be noted that the area of red $peak_{A+B}$ and $peak_{A+C}$ is much larger than that of red $peak_b$ and $peak_c$, indicating that there are other reactions over charge process, apart from the oxidation reactions of the I_3^-/I^- and I_2/I_3^- redox couples. Hence, two anodic peaks may also partly correspond to the oxidation reaction of the discharge products in the Li–air battery using 4 % SiO_2-LiI-GPE. These results demonstrate that the Li–air battery using 4 % SiO_2-LiI-GPE over the discharge/charge process shows better reversibility than the Li–air battery using 4 % SiO_2-GPE.

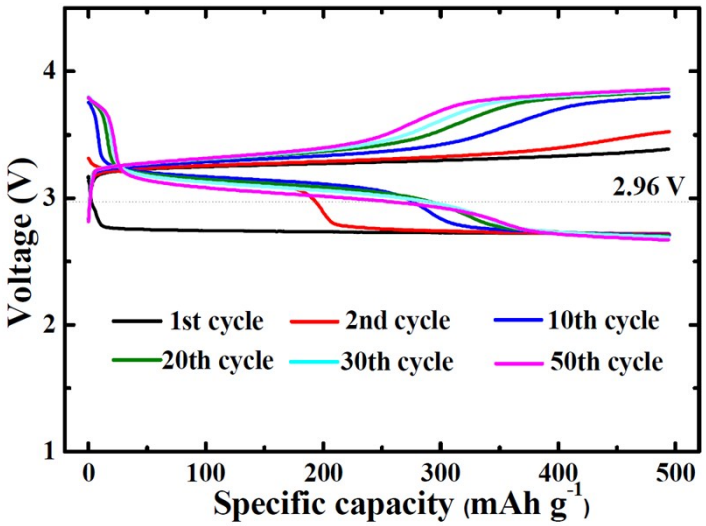

Figure S23 The discharge/charge curves of the Li–air battery using 4 % SiO_2-0.3 M LiI-GPE with rGO/Li anode at different cycles. The current density was fixed at 100 mA g^{-1} and the capacity was set at 500 mAh g^{-1}.

We have also prepared the GPE with 4 wt% SiO_2 and 0.3 M LiI (4 % SiO_2-0.3 M LiI-GPE), and further used it as electrolyte to assemble the Li–air batteries. As shown in **Figure S23**, the Li–air battery using 4 % SiO_2-0.3 M LiI-GPE with rGO/Li anode shows stable voltage curves with no capacity fade, but exhibits the gradually increased voltage polarization over 50 cycles. It is well known that the reduction potential of O_2 is < 2.96V. However, it should be noted that most of the discharge capacity (＞250 mAh g^{-1}) for the Li–air battery using 4 % SiO_2-0.3 M LiI-GPE with rGO/Li anode is obtained at the discharge potential of ＞2.96V after the first cycle, indicating that the main discharge reaction of this Li–air battery is not the reduction of O_2. Moreover, recent reports (**ref. S3-5**) have also demonstrated that the high concentrations of LiI can promote side reactions of the Li–air batteries, while the low concentrations of LiI (< 0.1 M) can serve as a redox mediator for Li–air batteries since the corresponding side reaction is negligible and the main reaction in these batteries is oxygen reduction/evolution reaction. Based on the above consideration, the high concentration of LiI additive is not really suitable for Li–air batteries.

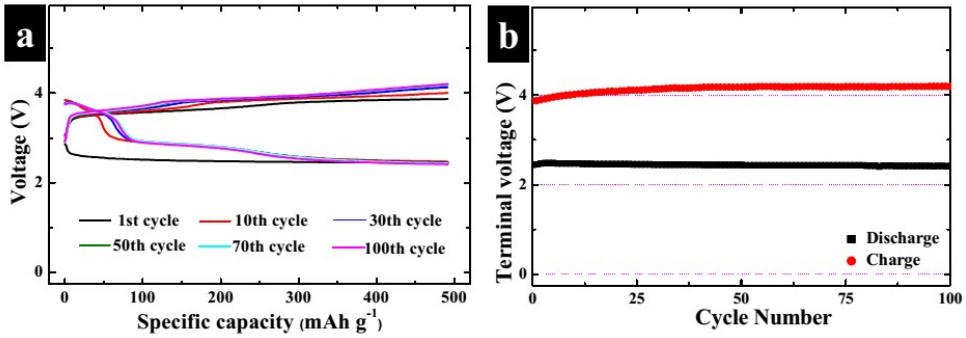

Figure S24 (a) Discharge/charge profiles of the conventional Li–air battery using 4% SiO_2-LiI-GPE with pure Li anode at different cycles in ambient air and (b) the corresponding discharge/charge terminal voltage versus cycle number. The current density was fixed at 100 mA g^{-1} and the capacity was set at 500 mAh g^{-1}.

As shown in **Figure S24a**, the voltage curves of the conventional Li–air battery using 4% SiO_2-LiI-GPE with pure Li anode are very reproducible for 100 cycles at 100 mA g^{-1} with a limited capacity of 500 mAh g^{-1}, except for a small voltage increase between the first charge profile and the following cycles. In addition, the Li–air battery using 4 % SiO_2-LiI-GPE with pure Li anode displays an average voltage gap of ~1.70 V over 100 cycles (**Figure S24b**), which is higher than that of the Li–air battery using 4 % SiO_2-LiI-GPE with rGO/Li anode (~1.45 V) at the same condition (**Figure 5e**). This result also indicates the superior Li plating/stripping performance of the rGO/Li anode.

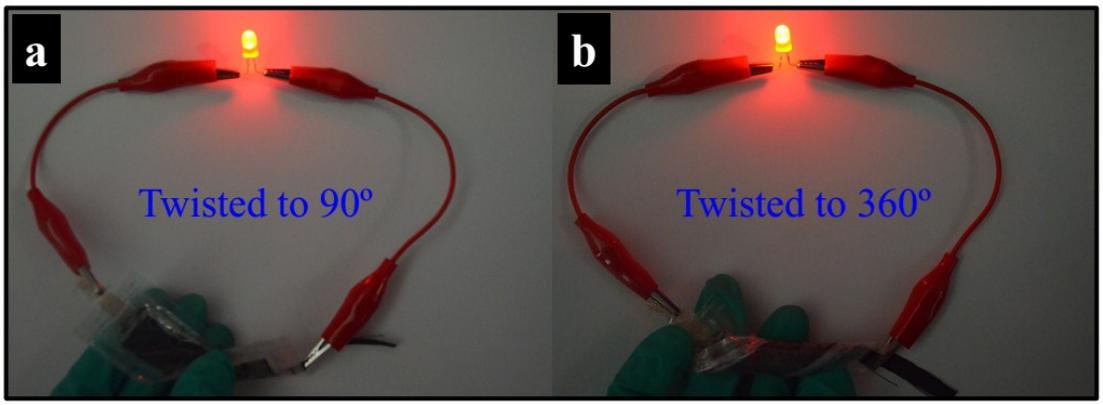

Figure S25 Photo profiles of a LED driven by a belt-shaped Li–air battery using 4 % SiO_2-LiI-GPE with rGO/Li anode at different bending conditions: twisted at degrees of (a) 90º and (b) 360º.

As shown in **Figure S25**, the belt-shaped Li–air battery using 4 % SiO_2-LiI-GPE with rGO/Li anode can also power a red light-emitting diode (LED) even under twist to 90° or 360º, further demonstrating the high mechanical strength and good electrochemical stability of this battery.

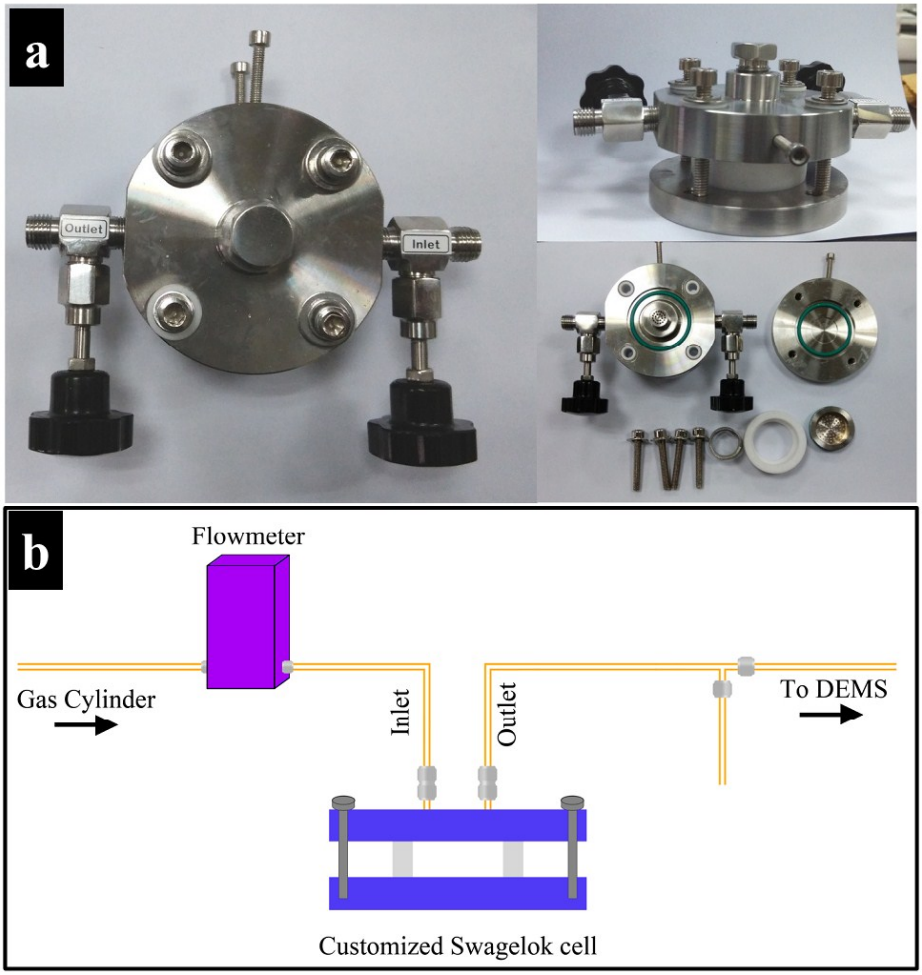

Figure S26 (a) Photo images of the customized Swagelok cell; (b)Schematic illustration of the DEMS analysis system.

The DEMS system was built in-house and guided by the requirement to detect the gases evolved during the charge. A quadrupole mass spectrometer (NETZSCH QMS 403 C) with leak inlet is connected to a customized Swagelok cell assembly (**Figure S26**). The cathode current collector is integrated with two tubes as purge gas inlet and outlet (**Figure S26**). When analyzing the gas evolution over recharge process of 4 % SiO_2-LiI-GPE based Li–air battery, the tested cell should be firstly discharged in the air. For each tested cell, the system was purged with a pure N_2 stream for 6 hours, and the background for O_2 and CO_2 was calibrated before the charge test and online gas analysis. Purge gas flows were typically 1 mL min^{-1}

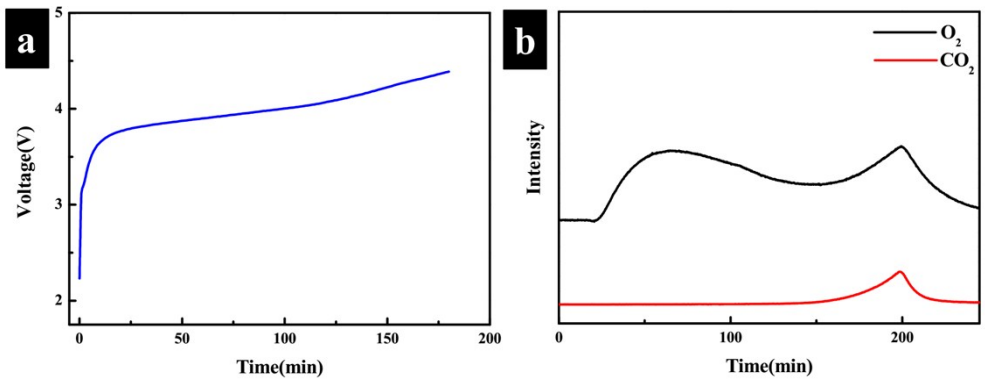

Figure S27 (a) The charge curve at the current density of 100 mA g^{-1} and at the fixed capacity of 1000 mAh $g^{-1}$and (b) corresponding gas evolution analyzed by *in situ* DEMS.

In situ DEMS measurement was also conducted to analyze the gas evolution over recharge process of the bulk Li–air batteries with rGO/Li anode using 4 % SiO_2-LiI-GPE. As shows in **Figure S27**, the evolution O_2 dominates the charge process which is accompanied by CO_2 evaluation.

Reference

ref. S1: W. S. Hummers and R. M. Offeman, *J. Am. Chem. Soc*., 1958, **80**, 1339.

ref. S2: W. Stöber, A. Fink and E. J. Bohn, *J. Colloid Interface Sci.*, 1968, **26**, 62.

ref. S3: Z. Y. Guo, C. Li, J. Y. Liu, Y. G. Wang and Y. Y. Xia, *Angew. Chem. Int. Edit.,* 2017, **129**, 7613.

ref. S4: W. -J. Kwak, D. Hirshberg, D. Sharon, H.-J. Shin, M. Afri, J. -B. Park, A. Garsuch, F. F. Chesneau, A. A. Frimer, D. Aurbach and Y. -K. Sun, *J. Mater. Chem. A*, 2015, **3**, 8855.

ref. S5: T. Liu, M. Leskes, W. Yu, A. J. Moore, L. Zhou, P. M. Bayley, G. Kim, C. P. Grey, *Science*, 2015, **350**, 530.